Moisture sensitivity and compressive performance of 3D-printed cellulose-biopolyester foam lattices.

John McDonald-Wharry[a*], Maedeh Amirpour[b], Kim L Pickering[a], Mark Battley[b], and Yejun Fu[c]

[a] *School of Engineering, The University of Waikato, New Zealand*

[b] *Centre for Advanced Composite Materials, The University of Auckland, New Zealand*

[c] *School of Design, Victoria University Wellington, New Zealand*

[*] Corresponding author: john.mcdonald-wharry@waikato.ac.nz

Graphical Abstract

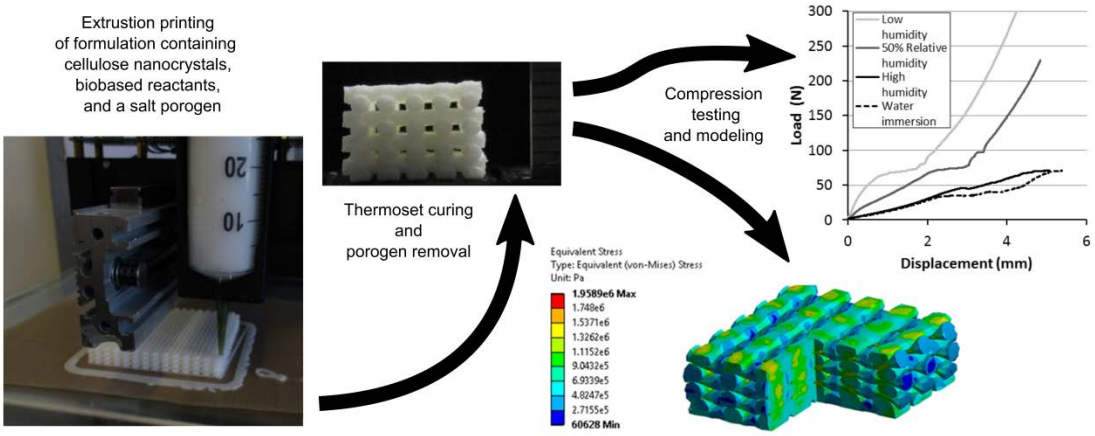

Abstract

Biobased, foam-like polyester composite materials were 3D-printed from a thermoset paste formulation composed of sebacic acid, glycerol, citric acid, and cellulose nanocrystals in water and ethanol with potassium chloride as a salt porogen. Thin walls and lattices were 3D-printed with geometry selected to facilitate post-printing processes such as water removal during polyester curing, and the post-curing removal of the salt porogen. The compressive performance of these moisture-sensitive lattice structures was investigated after conditioning at different humidity

levels and by water immersion. Finite element analysis was used to simulate the compressive performance of these porous lattice structures using a crushable foam material model. Addition of plant triglyceride oils from sunflower and coconut were trialled to modify the compressive performance and moisture sensitivity. Addition of 5wt% coconut oil to the formulation prior to 3D-printing was found to lower the cured material's stiffness under dry conditions while increasing the compressive plateau strength of the lattice structures after water immersion.

Keywords: Additive manufacturing, nanocellulose, polyester, foam, direct-write assembly

1. Introduction

Additive manufacturing technologies are often well-suited for fabricating open lattice, space frame, or thin-walled structures [1]. Such structures have a number of advantages compared to solid, monolithic structures such as reduced print times, lower material costs, and mass reduction for the manufactured objects. These open and thin-walled structures also have high surface-area-to-volume-ratios which can facilitate the use of diffusion-base production processes and surface treatments. Solvent evaporation and polyester curing with volatile condensation by-products are examples of processes that can benefit from thin, high-surface-area structures. The use of salt porogens in thermosets with post-curing leaching is often used for creating porous scaffolds or biomedical applications [2-5], and the leaching process benefits from high-surface-area structures. New formulations and fabrication approaches can be developed specifically for 3D-printing these open and thin structures and utilise post-printing processes which benefit from high surface-area-to-volume structures (drying, curing, diffusion-based component removals, or various surface treatments). However, some of these formulations and fabrication approaches have proven to be unsuitable for preparing the thick monolithic specimens which are the basis of standard mechanical testing procedures such as ASTM D1621. These new materials can be unsuitable for conventional manufacturing approaches such as casting because of problems such as blistering due solvent evaporation and release of water during curing reactions. In an effort to compare the mechanical properties of formulations unsuitable for fabricating thick, monolithic testing specimens, this work experiments with the fabrication and compressive

testing of lattice structures.

Simple “log-pile” lattice structures of extruded strands in stacked arrays are commonly found in the 3D printing literature [6-9] and are used across a diverse range of materials and application areas, including the direct-write assembly of ceramics [10, 11] and hydrogels used as cell culture scaffolds [3, 12]. Often used in trials of formulation printability [10, 13, 14], these “log-pile” lattice structures can be created via the rectilinear infill pattern feature on typical software used to generate the g-code toolpaths for 3D printers. In the current work, such “log-pile” lattice structures are printed, cured, made porous through salt porogen removal, cut into subsample specimens, conditioned as replicates, then tested under quasi-static compression testing to compare different formulation variants and evaluate how their performance changes with moisture uptake. Modelling of these lattice structures in compression was also investigated and was informed from smaller-scale compression and tensile experiments.

Cellulose-based materials and other bio-based polymers with polar chemistry tend to be water sensitive, often undergoing substantial changes in dimensions and properties with exposure to moisture, leading to major changes in structural geometry and mechanical properties [15, 16]. Such water-sensitivity in materials is a potential problem in a range of different applications [17], however this sensitivity is also potentially useful in the creation of responsive materials for 4D printing [18]. Establishing formulation assessment approaches and having a better understanding of the effects of moisture in 3D-printed biobased materials is important, whether the aim is to improve water-resistance for more stable performance in a range of

environments or enhancing water-sensitivity for engineering controlled 4D responses. In keeping with an overall aim to create 3D-printable formulations from biobased and bioderived reagents the, addition of triglyceride plant oils was trialled with the aim of adjusting both the compressive performance and the moisture sensitivity of the cured material. Coconut oil was chosen as an example of highly saturated plant oil and for comparison sunflower was chosen as an example of unsaturated plant oil. Coconut oil containing triglycerides largely composed of saturated fatty acids [19] was hypothesised to remain mostly unreacted during the curing process and act as a plasticiser in the cured material. Sunflower oil with a higher proportion of carbon-carbon double bonds (from unsaturated fatty acids such as linoleic acid) was hypothesised to be able to undergo oxidative cross-linking during the curing process [20], potentially providing a second, more water-resistant thermoset phase to the composite.

2. Materials and methodology

Cellulose nanocrystals in powder form were purchased from Celluforce™, Canada. Citric acid ($C_6H_8O_7$) crystals, glycerol ($C_3H_8O_3$, 99.7% USP grade), Sunflower (*Helianthus annuus*) oil, and refined coconut (*Cocos nucifera*) oil were purchased from Pure Ingredients Ltd, New Zealand. Sebacic acid (Decandioic acid, $C_{10}H_{18}O_4$) granules (99% purity) were purchased from Sigma-Aldrich. Ethanol, acetone and potassium chloride (each EMSURE® analysis grade), along with silica gel desiccant (granulate with orange indicator) were sourced from Merck KGaA, Germany.

2.1. Preparation of formulations

A base syringe-printable formulation was prepared by mixing the constituents in proportions outlined in Table 1. Distilled water, glycerol, citric acid and cellulose nanocrystals were mixed together, and stirred at 90-96°C for 40 minutes to form a shear thinning gel. Sebacic acid was dissolved in boiling ethanol then mixed into the gel which was then stirred at 90-96°C for a further 50 minutes (note that water and ethanol were evaporating during these steps). Potassium chloride salt (KCl) was ball-milled and passed through a 250µm sieve before being mixed into the formulation as a porogen filler. The resulting formulation was treated with two homogenisation steps (3 minutes at 3000rpm) on a benchtop homogeniser (Silversen L4RT) with manual mixing between steps before being stored in sealed containers and cooled. At this point the base formulation was found to lose 32% of its original mass after 1 hour in an oven at 105°C, and lost 41% of original mass with a 48 hour cure at 105°C. Two 85.5g samples of this base formulation were spatula-mixed with 4.5g of either sunflower oil or melted coconut oil to create the modified "+ sunflower oil" and "+ coconut oil" formulation variants each with 5wt% oil. Formulations were stored at 5±3°C, and warmed to room temperature prior to printing

Table 1: Base formulation

Constituent	Mass added, g	wt% (excluding water & ethanol)
Cellulose nanocrystals	42.9	11%
Citric acid	54.6	14%
Sebacic acid	101.4	25%
Glycerol	63.2	16%
Potassium chloride	141.2	35%
Ethanol	159.7	
Distilled water	193.6	

2.2. Syringe 3D printing of the formulations

The formulations were transferred to 60 ml syringes and printed through a tapered polypropylene tip (1.52mm ID, Jensen Global) on to a sheet of PTFE-coated glass fibre fabric (Dotmar Engineering Plastics). The same g-code toolpath was used to 3D print two lattice (or "log pile") structures (Figure 1a) from each of the three formulation variants. An SDS-60 Syringe Dispenser on an Engine-SR machine (Hyrel International, Inc) was used to carry out the 3D printing. The lattice g-code (Figure 1a) was generated from slicing a 63.4mm x 63.4mm x 10mm square prism in Slic3r software based on the following parameters: extrusion widths and layer heights set to 1.2mm, 40% rectilinear infill, 10mm/s printing speed, no perimeter shells (although with the overlap of infill with perimeter shell setting fixed at 100%).

A thin-walled box section structure was also 3D-printed (Figure 1b) from the oil-free base formulation. The square tube (or box section) structure was 80mm x 80mm x 6mm with walls composed of strands stacked 5 layers high and one strand wide.

Once cured samples were cut from the walls of the box section for small scale compression and tensile testing to inform the simulations.

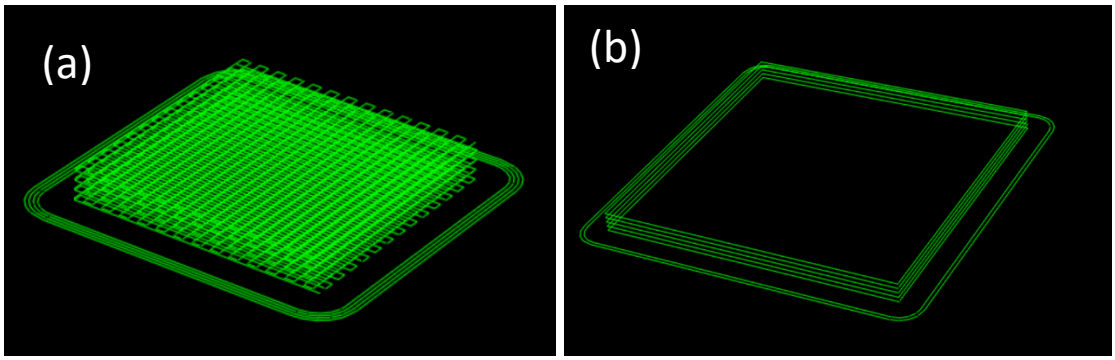

Figure 1: Representations of syringe printing g-code toolpaths for (a) "log pile" lattice structures and (b) the box section structure.

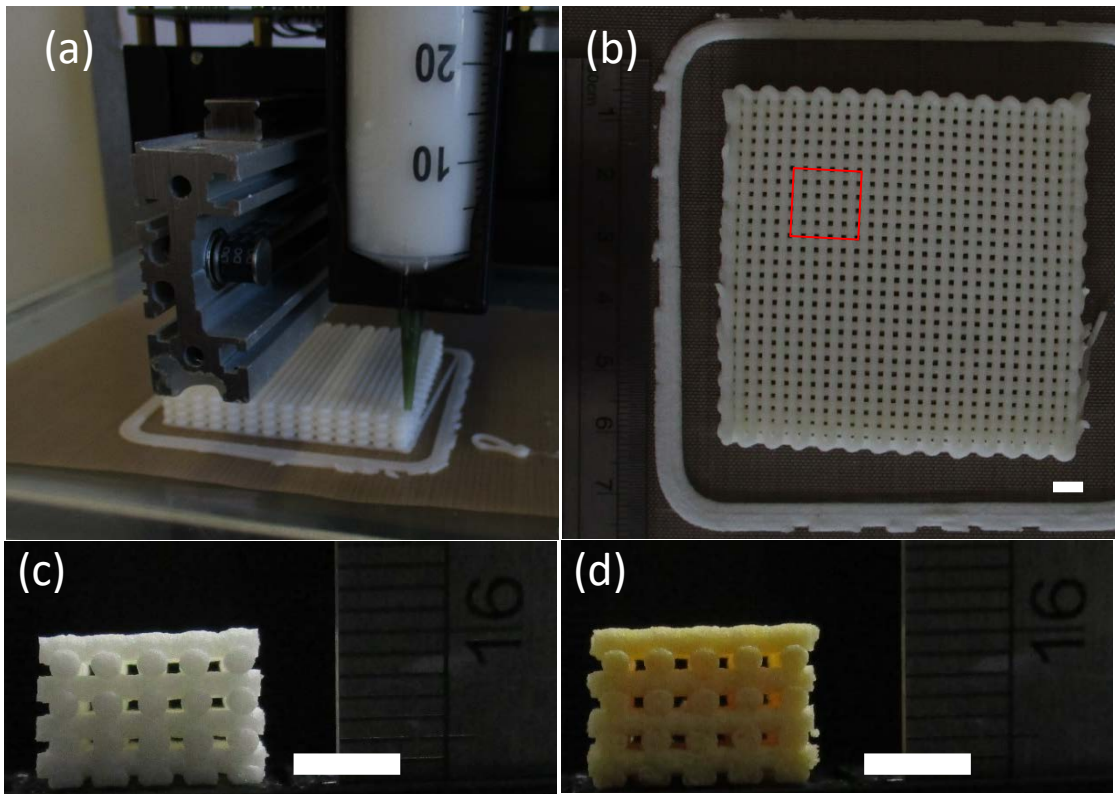

Figure 2: (a) Syringe printing of large lattice structure, (b) post-cure lattice structure with red box indicating cutting to create lattice specimens as replicates for condition and testing, (c) lattice sample of base formulation (d) lattice sample of base formulation + sunflower oil. White scale bars represent 5mm.

2.3. Post-printing treatments and conditioning

Printed structures (Figure 2a) were cured for 48 hours in a vented oven (105+2°C). Thermal curing involves a condensation reaction where glycerol, sebacic acid, and citric acid polymerise to form a polyester [21-23]. During curing ester bonds between the surfaces of the cellulose nanocrystals and the polyester matrix may also form. The polymerisation reaction produces water which is removed by the elevated oven temperature. Following curing, the lattice structures were immersed in distilled water (4 litres of water per 40g of cured material) for 24 hours to dissolve the potassium chloride and create the porous foam-like structure. Subsequently, the structures were rinsed with distilled water, cut into lattice specimens with a scalpel (specimens were approximately square based on cutting out 5 strands by 5 strands wide as indicated in Figure 2b), then dried in a vented oven for 20 minutes (105+2°C). These lattice specimens (Figure 2c,d) were then stored in sealed box with silica desiccant at 23°C for over 72 hours prior to the 48-hour conditioning steps. Four sets of lattice specimens (with 7 replicates) of each formulation variant were used to investigate how the compressive properties, weight gain (water uptake) and dimensional changes (swelling) would be influenced by four different conditioning environments. The sets of 7 lattice specimens were used as replicates for the conditioning experiment. The four conditioning environments where specimens were placed for 48 hours at 23°C were:

1. Low humidity (sealed container, specimens above silica desiccant)
2. 50% relative humidity (conditioning in a Binder constant climate chamber)
3. High humidity (sealed container, specimens above liquid distilled water)

4. Water immersion (sealed container, specimens held under distilled water)

Dimension changes were measured from digital photographs taken before and after curing of the printed lattice structures and before and after conditioning of cut lattice specimens. Compression testing was carried out in a room at 23°C and 50% relative humidity on lattice specimens within minute of the specimens being removed from the conditioning chamber.

2.5. Physical and mechanical characterisation

Scanning electron microscopy: Samples were mounted on carbon tape and coated in platinum using a Hitachi E1030 Ion sputter Coater prior to SEM images being recorded on a Hitachi S-4700 Scanning electron microscope. Scalped cut surfaces were imaged. To minimise issues with liquid oil, additional SEM images were recorded after the foam lattice samples were treated with boiling acetone. For the boiling acetone treatment 0.04g sub-samples of lattices were each immersed in 40mL of boiling acetone for 5 minutes, washed with 40ml of acetone, and allowed to dry (24 hours at room temperature followed by 20 min in a 105°C oven) prior to SEM analysis.

Compression testing of lattice structures

An Instron 33R4204 universal testing machine with a 5 kN static load cell was used to test the lattice specimens (5 replicates) in quasi-static compression. The speed of testing was 5 mm/min and the specimens were loaded in what was the z-axis during printing. A pre-test procedure closed the distance to specimens at 10mm/min and started recording data after the load reached 0.5 N.

Tensile and compression testing of walls and strands

To inform modelling of the lattice structure, foam samples were cut from 3D printed walls prepared from the base formulation. Quasi-static compression and tension were tests were carried out with a standard Instron 5567 testing device. Flat platen compression rigs for testing of single strand samples (cross section 1.4 mm×1.04 mm) were designed which included two extensometers to measure the compression displacement. A 1kN load cell was used and an initial 6N preload applied to the test-piece. The final compression ratio was 75% of the original thickness. The tensile test was carried out with a 10N load cell. For the measurement of strain, an optical extensometer was used. Figure 3 shows the compression and tension testing setups.

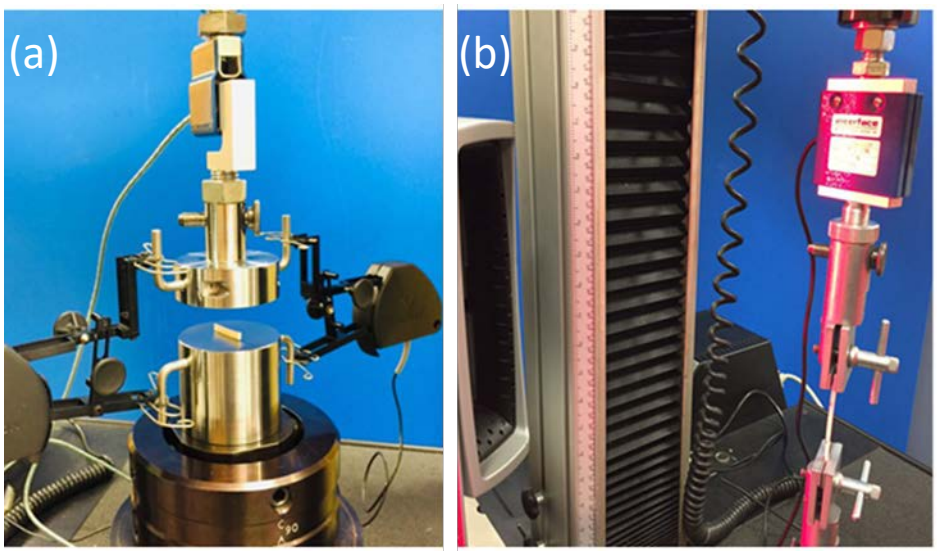

Figure 3: Compression (a) and tension (b) experimental testing setups

2.6. Foam and lattice deformation modelling

The foam and lattice finite element modelling was undertaken using ABAQUS/STANDARD Mechanical. An inverse calibration technique using

MCalibration software version 5.1.2 was used in combination with a FEA model of a single strand to determine an appropriate material constitutive model and input parameters for the foam which included permanent plasticity deformation under compression tests. This technique compares an FEA simulation of the test using ABAQUS version 2016 to the experimental data to fully characterise the behaviour of the material. Finite element (FE) simulation of the 3D-printed lattice structure (base formulation after 50% RH conditioning) was carried out using ANSYS static structural 19.2 package.

3. Results and discussion

3.1. 3D printability, curing observations and lattice density

The base formulation and those modified with plant oil addition were found to be printable into lattice structures which did not collapse post-printing or during the curing process (Figure 2). During drying and curing the printed structures underwent shrinkage. With 48 hours of cure the lateral shrinkage was greater in the oil-free base formation (-11.8±0.5%) than formulations with coconut oil addition (-8.6±0.8%) or sunflower oil addition (-6.5±0.4%), with significant differences in cure shrinkage found between all formulation variants. Slight yellowing had occurred during curing in the base formulation and the formulation with coconut oil addition. In contrast, the formulation with added sunflower oil underwent considerable yellowing and browning during the curing process, assumed to be related to reactions involving the unsaturated fatty acids present on the sunflower lipids [20].

Bulk densities of the dry lattice structures after the salt removal step were calculated

as 0.53g/cm^3 for the base formulation material, 0.54g/cm^3 for the material with added coconut oil and 0.51g/cm^3 for the material with added sunflower oil (standard deviations in these values were 0.02-0.03 g/cm^3 indicating little difference in lattice bulk densities).

3.2. Dimensional changes and water uptake during conditioning

The weights of specimens from all three formulation variants increased with higher humidity conditioning with the greatest weight increases occurring found water immersion conditioning (Table 2). The specimens with added sunflower oil had the highest water uptake with full water immersion. A small (<1wt%) weight loss in the specimens with the low humidity conditioning in the desiccant chamber indicated that the specimens had some moisture content prior to the start of conditioning. After high humidity conditioning, specimens with added coconut oil exhibited the lowest water uptake. Dimensional increases were on average between +3.1% and +7.5% for specimens conditioned in high humidity or with water immersion (Table 2) and length increases were found to be smaller than measured height increases (length increases averaging around 56% of the observed sample height increases). Although these swelling results had relatively large standard deviations (Table 2), they indicate significant anisotropy in the swelling of the 3D-printed structures, potentially resulting from the printing process aligning cellulose nanocrystals within the composite along the printing direction. This swelling anisotropy was less pronounced than that previously reported for 3D-printed lattice structures printed from cellulose nanofibril-reinforced hydrogels by Sydney Gladman et al [18].

Table 2: Dimensional changes and weight changes after conditioning for 48 hours at 23°C

	Low humidity	50% Relative humidity	High humidity	Water immersion
Height changes				
Base formulation	+0.08% (1%)	+0.03% (1.3%)	+8.8% (1.6%)	+7.5% (2.1%)
Base formulation+coconut oil	+0.7% (0.8%)	+0.9% (1.3%)	+7.9% (1.4%)	+6.5% (1.4%)
Base formulation+sunflower oil	+0.9% (1.4%)	+1.1% (1.1%)	+5.0% (2.1%)	+6.3% (2.3%)
	Low humidity	**50% Relative humidity**	**High humidity**	**Water immersion**
Length changes				
Base formulation	+0.1% (1.4%)	-1.8% (1.7%)	+5.7% (2.4%)	+3.9% (1.7%)
Base formulation+coconut oil	+1.1% (0.7%)	-0.2% (1.1%)	+4.2% (1.2%)	+4.1% (1.3%)
Base formulation+sunflower oil	+0.7% (1.1%)	+0.5% (1.1%)	+2.7% (1.7%)	+3.2% (1.1%)
	Low humidity	**50% Relative humidity**	**High humidity**	**Water immersion**
Weight changes				
Base formulation	-0.5% (0.1%)	+2.2% (0.2%)	+18.5% (0.6%)	+51(3%)
Base formulation+coconut oil	-0.5% (0.1%)	+2.02%(0.06%)	+16.0% (0.4%)	+48% (2%)
Base formulation+sunflower oil	-0.8% (0.2%)	+1.8% (0.5%)	+17.5% (0.6%)	+71% (3%)

Values in brackets represent 1 standard deviation from measurements of 7 replicates

3.2. Mechanical testing

Example quasi-static force-displacement curves for the lattice specimens under compression (Figure 4) had major regions which resemble the regions identified in other foams. In typical foam materials these three regions are known as the pseudo-elastic region (at low displacements), the plateau region, and a densification region

(found at high displacements) [24]. Additional features (resembling sharper increases in load and smaller plateaus) on the force-displacement curves were often observed at the beginning of the apparent densification region and may result from the failure or collision of parts of the lattice structure and higher strains. These additional features may also result from partial plastic collapse of foam cell walls because the failure is localised in a band transverse to the loading direction. When the cells have almost completely collapsed the opposing foam cell walls touch and further strain compresses the solid itself. Multiple gradients were also observed in the load-displacement curves before the plateau, complicating the analogy with traditional foam compressive behaviour. Structural stiffness values (Figure 5a) were calculated from the maximum slope occurring below 1 mm displacement on the force displacement graph then converted to engineering stress and strain values assuming a square prism for the bulk lattice structure based on the outer dimensions of the lattice structure tested. Values for stress at 10% strain (Figure 5b) were calculated based on the ASTM D1621-10 approach [25]. That standard calculates a 'compressive strength' at 10% strain unless a stress maximum has occurred at a lower strain value. However, these lattice structures tended to yield or reach a distinct plateau at much higher strains (20-55%) and the 'stress at 10% strain' values had a close correlation with the 'structural stiffness' values (Figure 5a). Compressive 'plateau strength' values for the lattice structures (Figure 5b) were calculated as the maximum stress occurring before the end of the main plateau region. The end of the plateau region in these lattice specimens was often seen as sharp increases in stress before typical foam densification occurs.

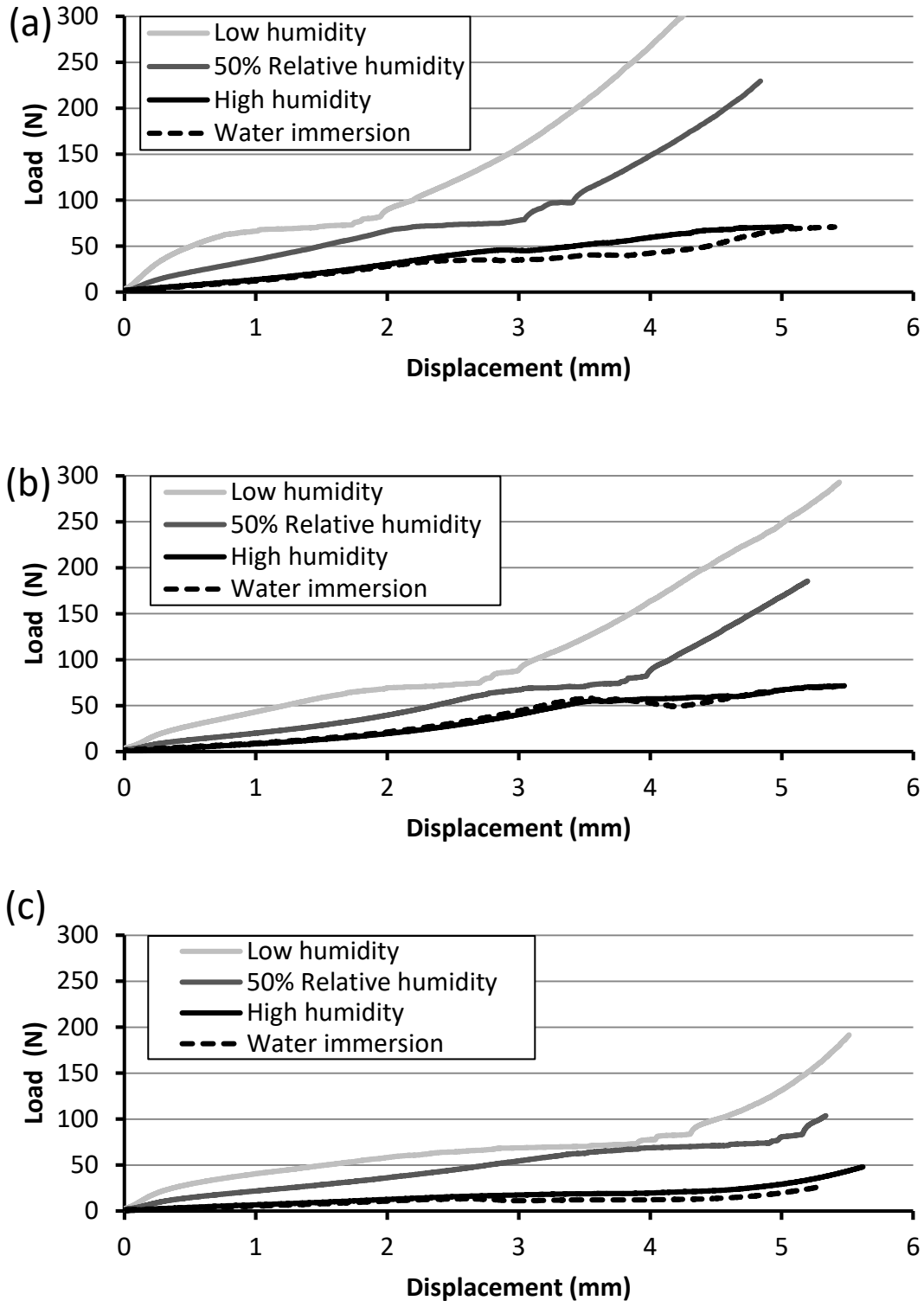

Figure 4: Example force-displacement plots from lattice sample compression for (a) base formulation, (b) base formulation +coconut oil, (c) base formulation + sunflower oil.

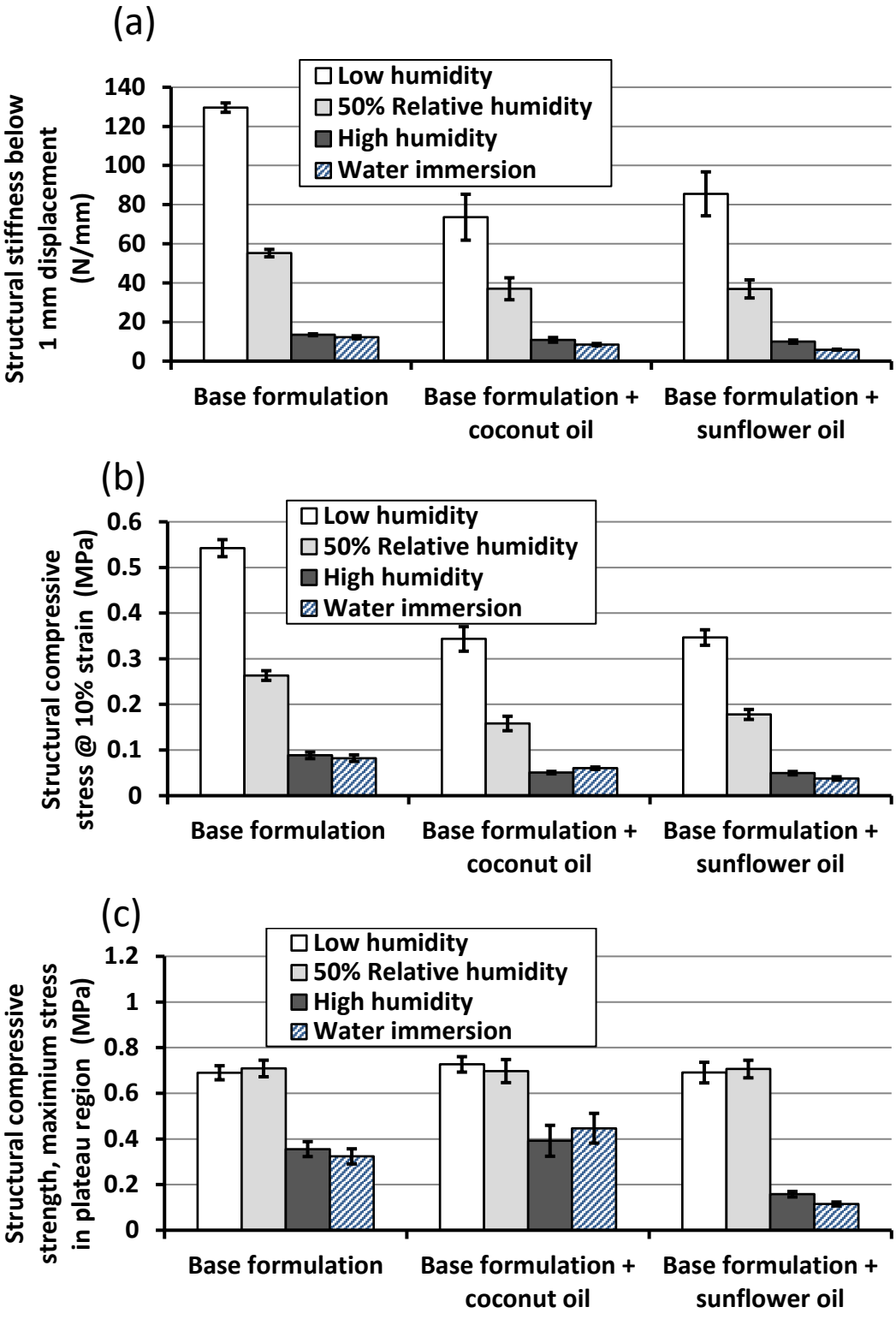

Figure 5: Lattice structural performance for formulation variants under conditioning at 23°C for 48 hours, (a) structural stiffness below 1 mm displacement, (b) compressive stress at 10% strain, (c) compressive strength as maximum stress in plateau region. Error bars represent 1 standard deviation from 5 replicates.

The compressive performance of specimens from all three formulations were highly sensitive to moisture content, demonstrating considerably lower stiffness (Figure 5a and Figure 5b) and lower plateau strengths (Figure 5c) after 48 hours of exposure to high humidity or water immersion when compared to 48 hours of standard conditioning (50% relative humidity, 23°C) or the low humidity conditioning in a container of desiccant.

The addition of either coconut oil or sunflower oil to the base formulation resulted in materials with decreased stiffness (-30-40%) at lower moisture levels when compared to the oil-free base formulation (Figure 5) indicating the oils can act as an alternative plasticiser to water at lower moisture levels. The sunflower oil addition results in a material which loses considerably more plateau strength than the oil-free base formulation with water immersion, suggesting that the sunflower oil addition interferes with the polyester cross-linking resulting in a weaker material. In contrast, coconut oil addition appeared to slightly improve the plateau strength of specimens conditioned with water immersion. Of the desiccant-dried specimens from the low humidity conditioning, those with added coconut oil were more resistant to damage during the compression testing (Figure 6). In contrast the specimens from the formulation with added sunflower oil underwent major damage during the compression testing, indicating the sunflower oil introduced weakness and brittleness to the composite material.

Figure 6: Low humidity conditioned specimens after compression testing of 5 replicates, (a) base formulation, (b) base formulation +coconut oil, (c) base formulation + sunflower oil.

To inform the initial modelling, compression and tensile tests were conducted on specimens of the base formulation cut from 3D-print thin wall structures and conditioned at 50% relative humidity. Figure 7a shows example experimental compression and tension engineering stress-strain results of the foam at strain levels of less than 10%. Cyclic tensile tests were undertaken which confirmed that the material showed elastic behaviour to this strain level.

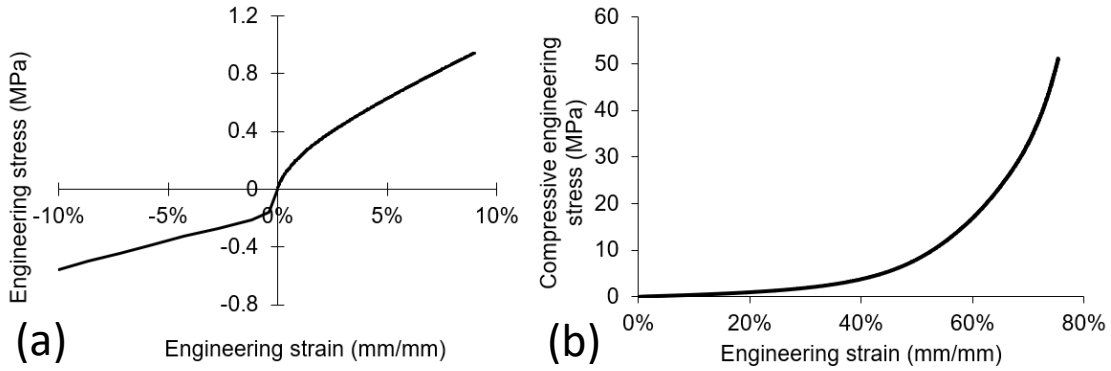

Figure 7: Engineering stress-strain curves for a single strand (a) compressive and tensile results between -10% and +10% strain levels, (b) compressive testing results to 75% strain. Base formulation after 50% relative humidity conditioning.

As seen from Figure 7a and Figure 7a, the deformation of the foam strand exhibits the three known regions which occur during uniaxial compression of foams: initial elastic deformation below approximately 10% of strain, collapse deformation with a sloping plateau to around 45% strain, and then rapidly increasing stiffness due to densification [26]. The initial elastic region of the compressive loading curve is attributed to cell wall bending. The sloping collapse plateau can be interpreted as involving elastic buckling and/or plastic yielding of cellular structures [27] which can absorb a considerable amount of specific energy. When the foam's cells have almost completely collapsed densification occurs, resulting in a significant increase in compressive stress with further strain [26-28].

3.3. Modelling and simulation

Three material models from ABAQUS were investigated (hardening plasticity [29], hyperfoam [24, 30] and crushable foam [27, 31]) and of these the crushable foam model with volumetric hardening proved to be the most accurate for this material. The crushable foam is a material property that, unlike hyperfoam, models the plasticity of a material as well as the densification region. The inputs to this model

therefore focus on the material's plasticity by requiring the plastic Poisson's ratio and yield stress and uniaxial plastic strain from the point of plasticity to densification. The compression yield stress ratio and hydrostatic yield stress ratio are also needed. Figure 8a compares experimental data and crushable foam material model obtained by an inverse calibration technique, using an FEA model of a single strand. It was found that the FE modelling predicted solutions exhibits fairly close agreement with those values obtained from experimental with a maximum relative error smaller than 10% at 0.4 mm displacement. The error increases to 20% at 0.75mm displacement. Possible causes of the error include variability in the cross-sectional geometry of the experimental specimens and frictional effects. Figure 8b shows the total deformation of the foam strand from the FEM solution up to 75% of compressive strain using the crushable foam material model obtained by the inverse calibration technique. The crushable foam model does not explicitly include the effect of porosity which will of course affect the mechanical properties of the printed material, however the use of an inverse calibration approach from a single strand for determining the input parameters means that these effects will be captured to some extent.

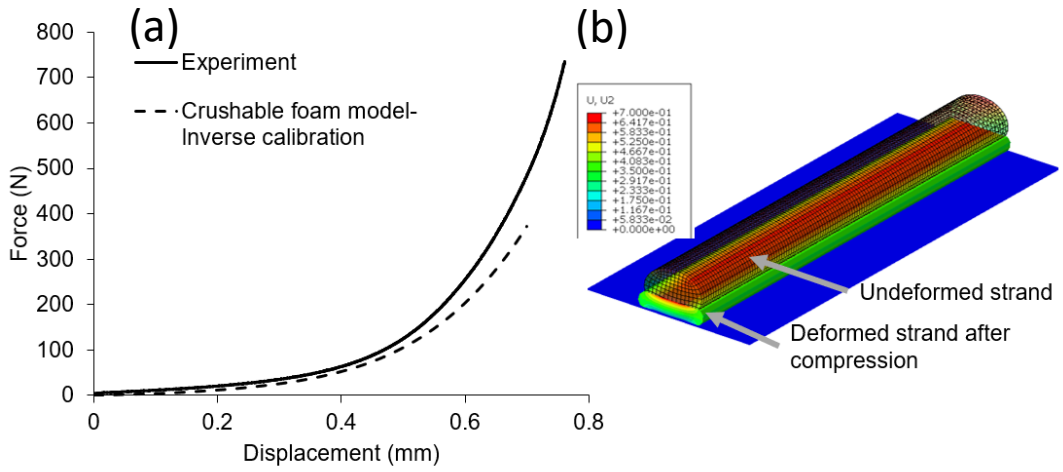

Figure 8: (a) Comparison between uniaxial compression experimental data and crushable foam material model obtained by inverse calibration technique. (b) Total deformation in loading direction of foam strand under 70% of compressive strain from ABAQUS FE solution and legend units are mm.

Finite element (FE) simulation of the 3D-printed lattice structure was carried out for the base formulation after 50% RH conditioning. The indenter and the base were modelled as isotropic structural steel with a Young's Modulus of 200 GPa and a Poisson's ratio of 0.3. The foam materials were modelled with an ABAQUS Crushable Foam plasticity model. All strands in the lattice structures were assumed bonded together (self-contact) to avoid possible collapse of the lattice if it comes into contact with itself. Augmented contact surface–surface algorithms were imposed at all material interfaces. The elements used were of type Tet4 linear elements with dimensions of approximately 0.1mm giving a total of approximately 39,000 elements. Due to large deflection and distortion in FE simulation and in order to improve the accuracy of simulation results, mesh nonlinear additivity approach with

skewness 0.9 was applied. Figure 9 shows the FEA von Mises stress and plastic strain distribution for the deformed lattice structure with 50% RH base formulation under 3 mm compression displacement. It can be seen that compressive forces were sustained by cross over points of two strands which have the greatest stress. In contrast, free sections without any contact with other strands experienced low level of stress and plastic strain.

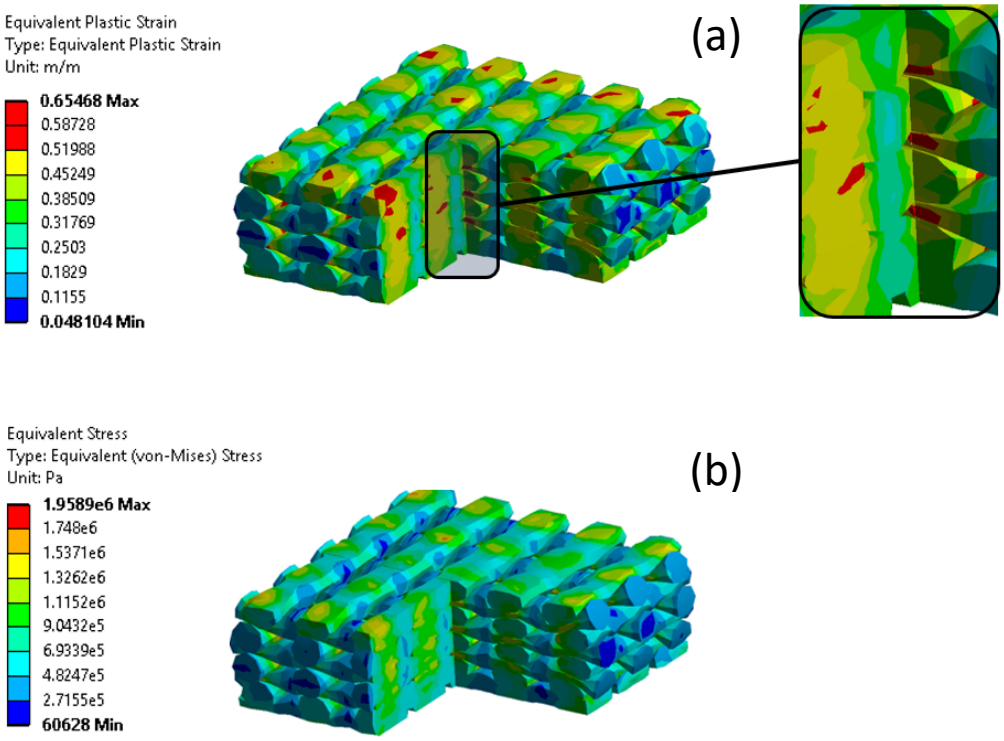

Figure 9: FEA simulation of "log-pile" lattice structure under 3mm compression deformation, Colours indicates (a) plastic strain and (b) von Mises stress

Force-displacement data from compression experimental test of the base formulation (50% relative humidity conditioning) is compared with FE simulation results predicted by the crushable foam material model in Figure 10. The FE simulation results are given up until a maximum displacement of 3.8mm because of

convergence issues due to extensive local nonlinear deformation beyond this point. It can be seen that the calibrated crushable foam model features all three regions and follows the experimental load–displacement response until approximately 50% of strain, however the initial elasticity deformation (region 1) exhibited a higher stiffness than found in experimental data and the simulated force/displacement slope over the 1-2mm displacement range was shallower than that found in experimental data.

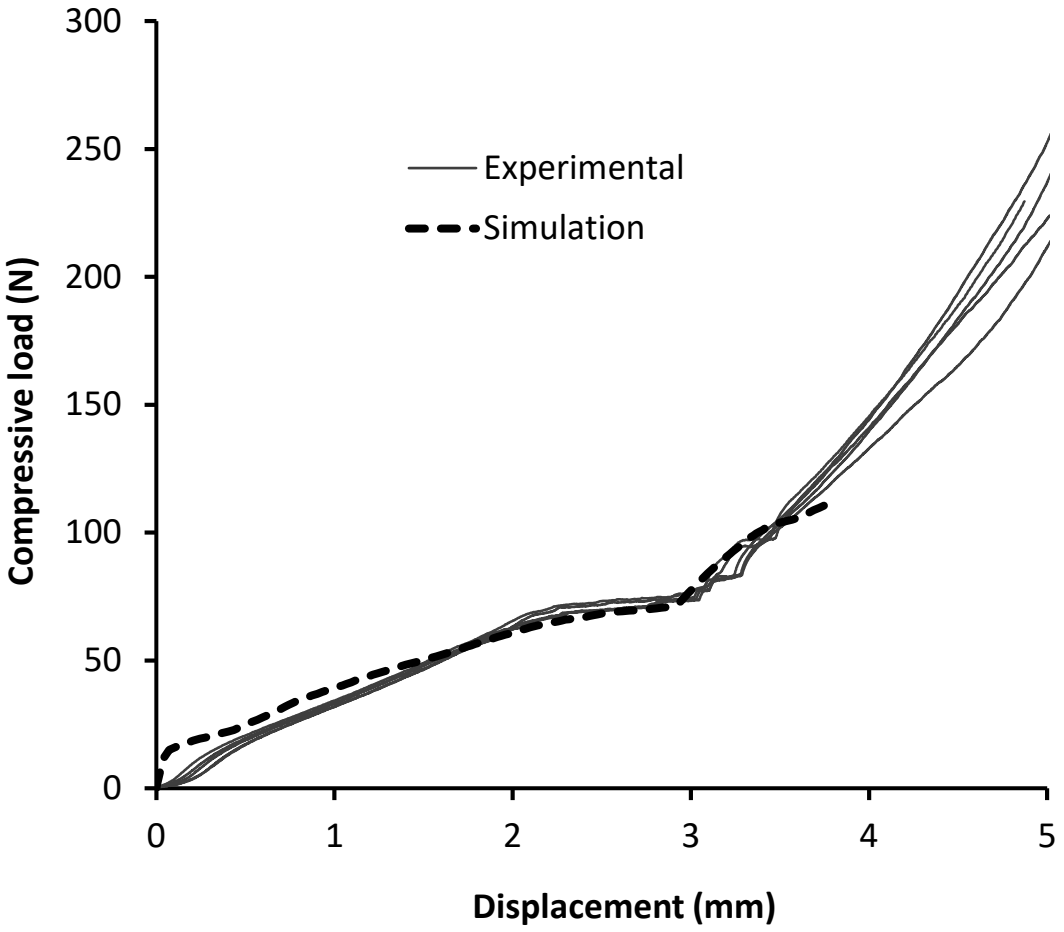

Figure 10: Load-displacement response of "log-pile" lattice structure under compressive loading, base formulation at 50% relative humidity. Simulation result compared to 5 experimental replicates.

The value for structural compressive stress at 10% strain (base formulation after, 50% relative humidity conditioning) was determined by the simulation to be 0.31 MPa which is higher than the experimental test which averaged 0.26 MPa. The FE simulation generated a value for plateau strength of 0.65MPa which was close to 0.67-0.76 MPa values obtained from experimental results (Figure 5c). For a lattice, the size of the voids will of course affect the stiffness and strength with a denser lattice of smaller voids having higher strength and stiffness. The ability of this printing approach to tailor both the material behaviour and the lattice geometry provides important opportunities to tailor the overall response as needed.

3.4. Scanning electron microscopy

The foams exhibited cuboid pores from the removal of the KCl salt crystals (Figure 11). At higher magnification (Figure 11d), particles with diameters around 80 nm could be observed protruding from broken foam walls and these resemble SEM images previously reported for a thermoset matrix reinforced with dispersed cellulose nanocrystals [32]. The foams prepared from the formulation with added coconut oil presented problems with SEM imaging due to liquid oil being present. In contrast, the foam specimens from formulations with added sunflower oil did not have this problem indicating the sunflower oil reacted during curing to form a solid. A boiling acetone treatment was conducted on lattice specimens prior to further SEM imaging. This acetone treatment resulted in weight losses (-15% from the oil-free lattice specimens, -30% from the lattice specimens with coconut oil and -35% from the lattice specimens with sunflower oil). The specimens cured from the oil-containing formulations had greater weight removals with the acetone treatments

indicating that this treatment removes the oil related phases. When compared to the base formulation lattice sample (Figure 12a), larger numbers of finer voids (on the order of 10 μm across) were observed in samples from the lattices with added coconut oil (Figure 12b) and sunflower oil (Figure 12c) after the acetone treatment. Two prominent types of surface textures could be observed at higher magnifications on samples in the base formulation lattices (Figure 12d). One is a rough surface with what appeared to be protruding particles or nodules and the second is a smooth surface. Assuming the rough surface is related to the presence of dispersed cellulose nanocrystals in a matrix (a similar texture to what has been reported for CNC dispersed in thermoplastics [33, 34]) then the smooth surface could relate to what was a phase with high sebacic acid content which contained no cellulose nanocrystals prior to curing. During curing the cellulose nanocrystals are expected to be relatively immobile in contrast to the diffusing polyester monomers/oligomers and this is hypothesised to result in these smooth regions remaining free of cellulose nanocrystals in the cured material. Smooth regions remain after acetone treatment in the base formulation lattices (Figure 13a,b). In contrast, smooth regions appear to be removed by acetone in the case of the lattices with added sunflower oil (Figure 13c,d) indicating that the smooth regions are inadequately cured in the presence of sunflower oil.

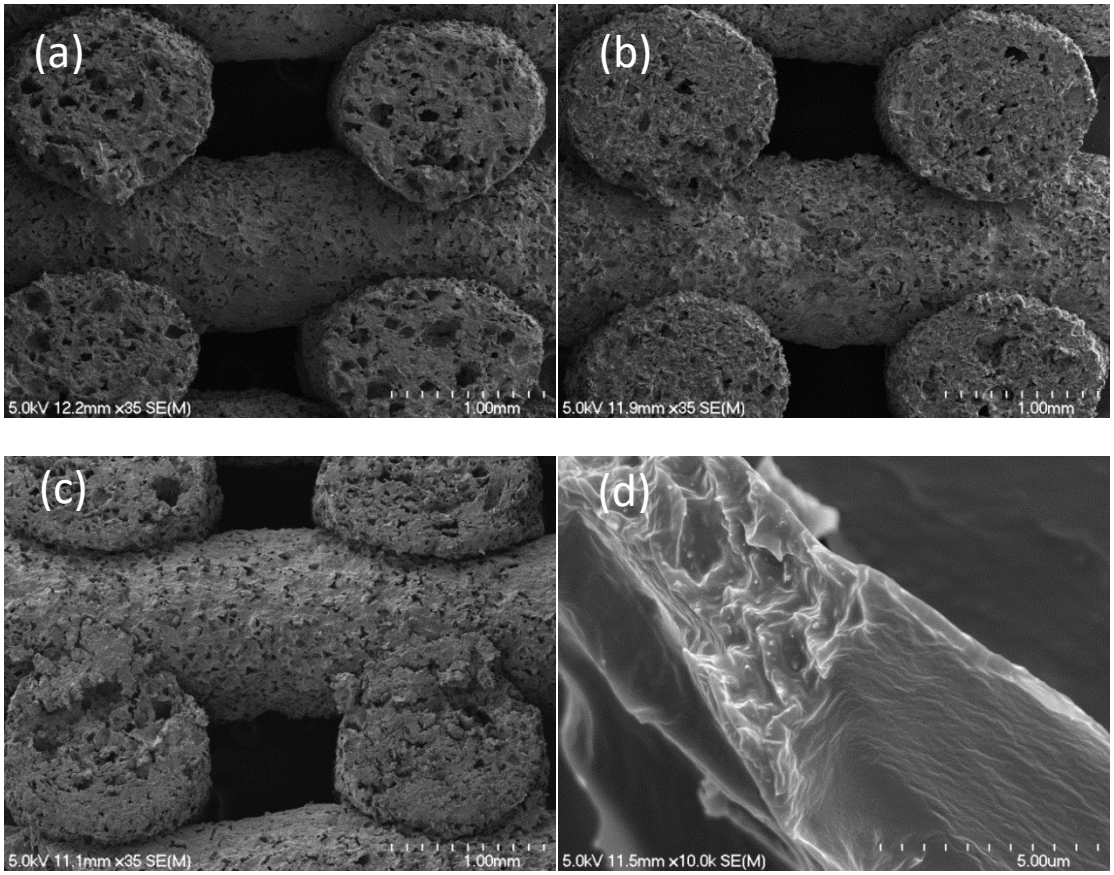

Figure 11: Scanning electron microscope images of lattice specimens, (a) base formulation, (b) base formulation + coconut oil, (c) base formulation + sunflower oil, (d) base formulation + sunflower oil at 10,000× magnification.

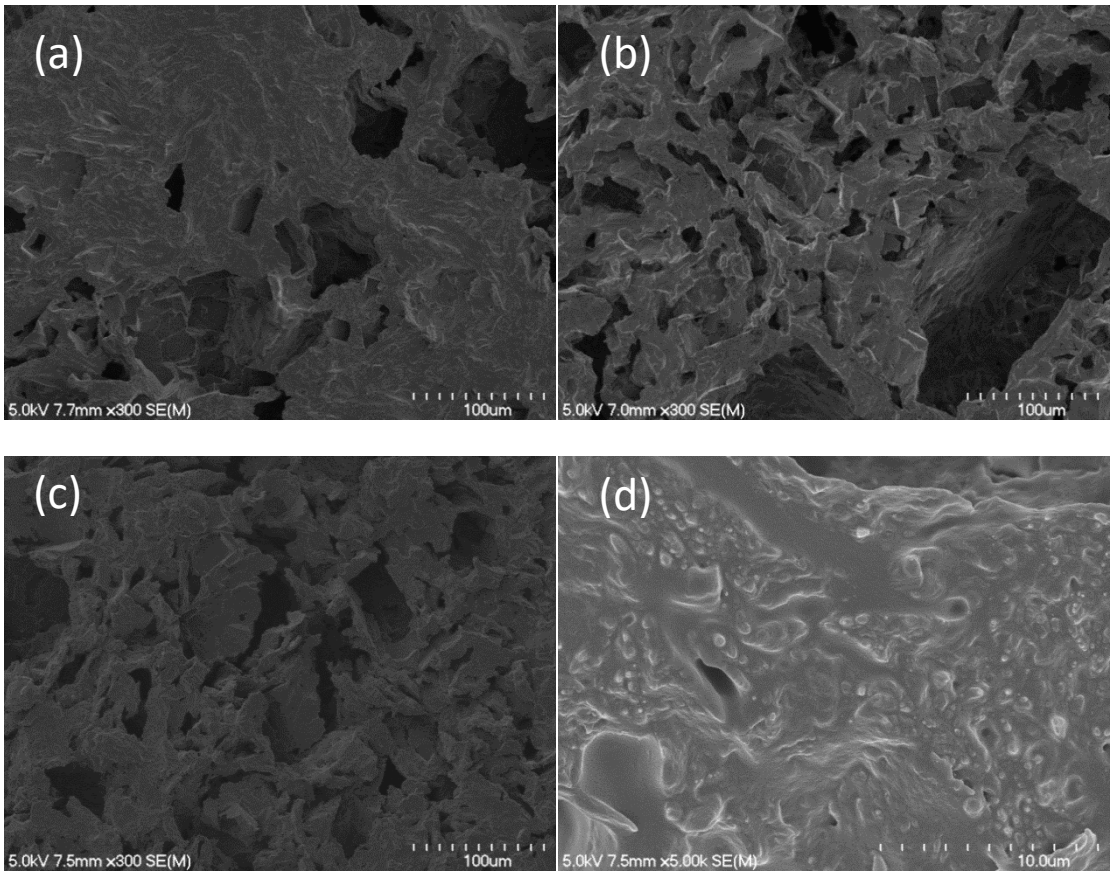

Figure 12: Scanning electron microscope images of samples from lattice specimens after acetone treatment, (a) base formulation, (b) base formulation + coconut oil, (c) base formulation + sunflower oil, (d) base formulation at 5000× magnification.

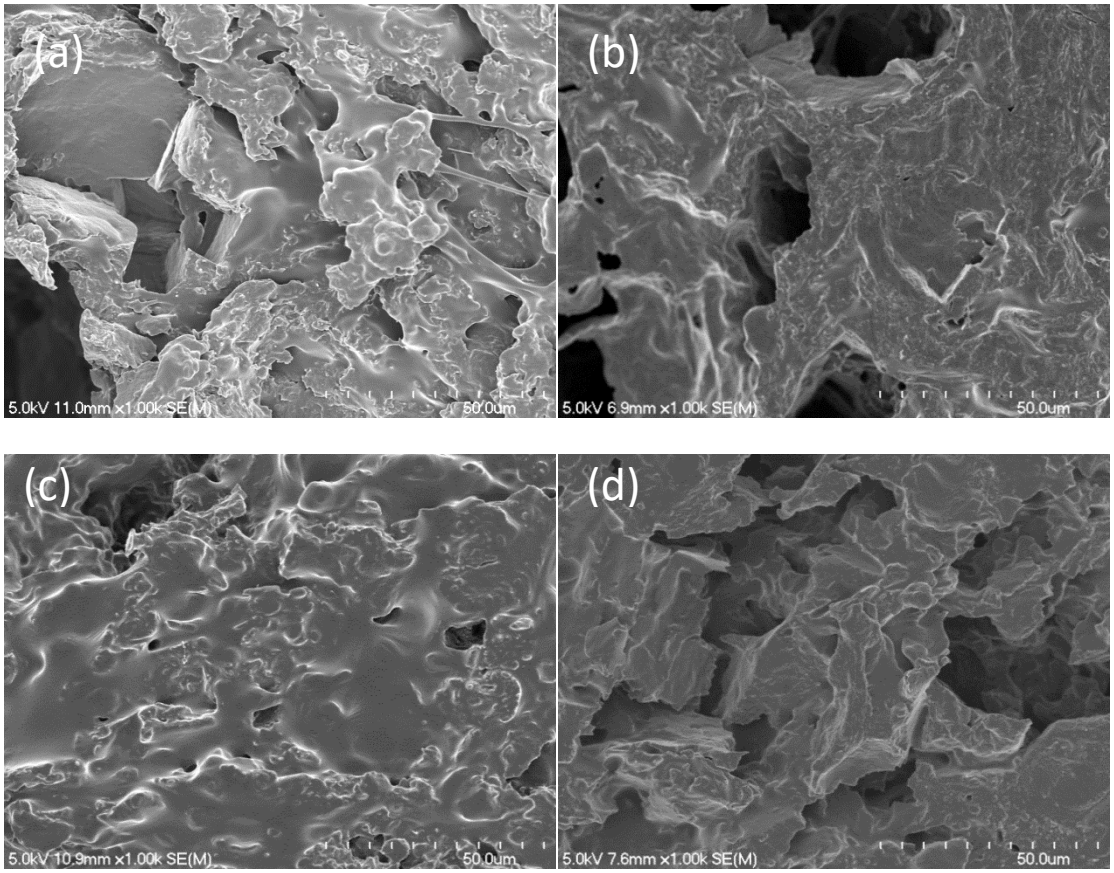

Figure 13: Scanning electron microscope images of samples from lattice specimens comparing surfaces with and without acetone treatment, (a) base formulation, (b) base formulation after acetone treatment, (c) base formulation + sunflower oil, (d) base formulation + sunflower oil after acetone treatment.

3.5. Further discussion and demonstration

To demonstrate the production of larger and more complex foam structures using this approach with biobased formulations an 'elbow guard'-size design was printed (Figure 14). This object exceeded 65mm in build height above the print bed without collapse and could be printed in approximately 30 minutes at a printing speed of 15 mm/s from one 60mL capacity syringe. Additional KCl was added to mitigate

collapse risk when printing this higher structure and to improve dimensional stability during curing, with the salt content (on a water & ethanol free basis) increased to 44wt% from the 35wt% used in the base formulation (
Table 1). 3D printing thermoset formulations containing NaCl salt as a porogen has recently been demonstrated by Lei et al. [3] and they also note the benefits of the salt in reinforcing the uncured structures. In the current work printable formulations which are sufficiently stable during curing are achieved through the use of both cellulose nanoparticles and KCl salt microparticles, allowing lower salt loadings to be used. CNC gel formulations also allow water and ethanol to be used to maintain extrudability of the paste, providing additional variables for optimising printability generally.

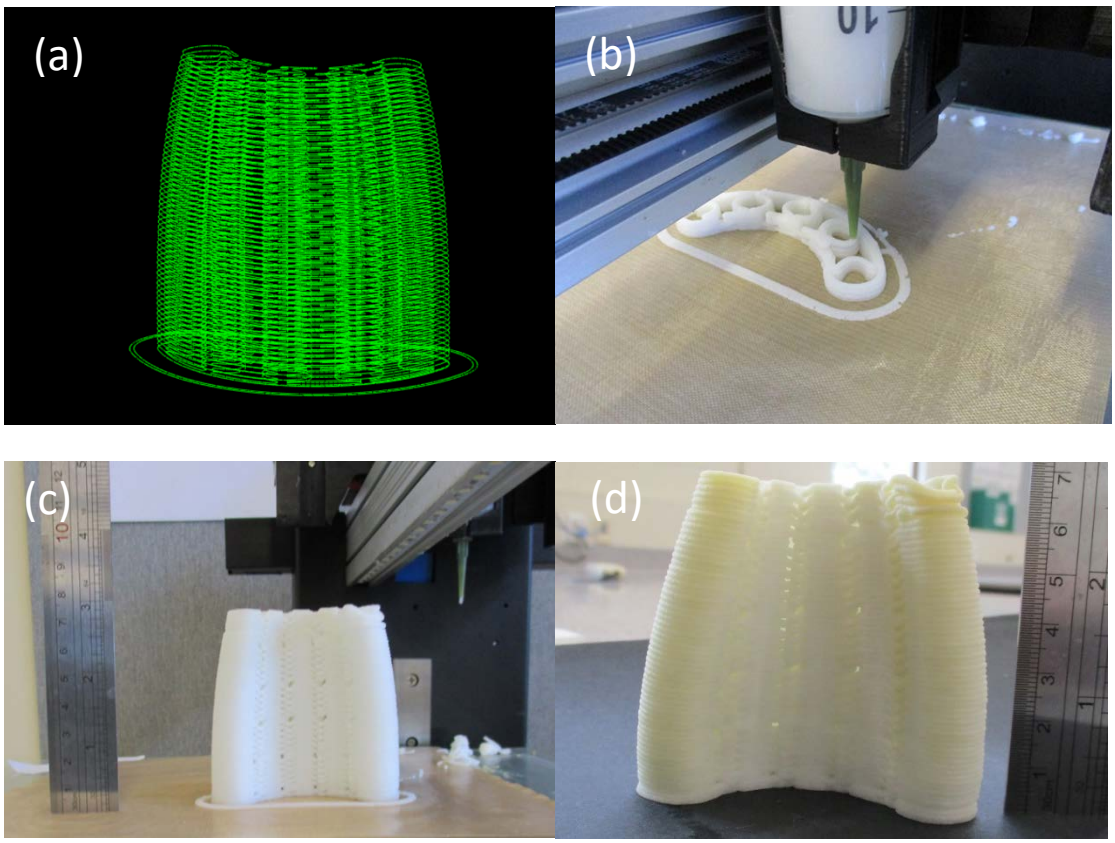

Figure 14: 3D printing an 'elbow guard' foam demonstrator object from base formulation + coconut oil with salt content increased to improve dimensional stability, (a) g-code toolpath for the design, (b) early stages of 3Dprinting, (c) post-printing and pre-curing, (d) final object after curing and salt removal.

3D printing foams and complex structures with foam-like compressive performance may have future applications in customised protective equipment, orthotics and other cushioning or wearables-type applications, moving beyond the tissue scaffold-type applications for which syringe-printed gels are often investigated. There is scope to customise both formulation and printed structure to engineer specific compressive performances and responses to applied pressure or impact and this is where modelling capability will be useful. In the case of biobased formulations,

improved control of moisture sensitivity will be important in future developments along with improving the specific mechanical performance of the materials to make them more comparable to conventional foam materials. Selection of application areas where moisture sensitivity is tolerable or advantageous is another option for further development.

4. Conclusions

Biobased thermoset polyesters composed of citric acid, sebacic acid, glycerol and cellulose nanocrystals can be 3D-printed via a syringe-based extrusion approach. These polyesters, with high biobased/bioderived material contents, can be converted into foam-like materials through the pre-printing addition of a salt porogen and removal of this salt using water after curing.

The compressive performance of this material is highly sensitive to moisture content, having reduced stiffness (-78%) and plateau strength (-54%) after 48 hours of water immersion when compared to 48 hours of standard conditioning (50% relative humidity, 23°C).

The addition of either coconut oil or sunflower oil to the base polyester and KCl formulation resulted in materials with decreased stiffness (-30-40%) at lower moisture levels when compared to the oil-free base formulation. In the case of coconut oil this reduced stiffness is interpreted as due to the oil acting as an alternative plasticiser to water and liquid oil inclusions remaining in the cured material. Like the oil-free material, the material with coconut oil also loses considerable stiffness and strength when exposed to high humidity conditioning or water immersion, however the loss of plateau strength with water uptake is smaller

with the coconut oil addition. In contrast, sunflower oil addition resulted in a weaker material and greater loss of plateau strength with water uptake. Sunflower oil addition also resulted higher water uptake during immersion and greater mass loss if extracted with boiling acetone indicating that sunflower oil also interfered with the polyester curing reactions.

"Log-pile"-type lattice structures, which are commonly prepared in additive manufacturing research, can be compression tested in order to provide measurements for comparing formulations under development and evaluate their relative sensitivity to environmental factors such as humidity. However, these lattice structures have complex behaviour in compression and further investigation into more suitable standardised structures is needed. Modelling the compressive response of these foam-like lattices is possible though finite element analysis and this can inform future engineering of 3D-printed foam-like structures for specific responses to compressive deformation. Moreover, predictive computational models could be utilised to address how moisture sensitivity and geometrical variations within such lattice structures influence their mechanical performance.

Acknowledgements

This work was supported by funding from the New Zealand National Science Challenge: Science for Technological Innovation - Kia kotahi mai - Te Ao Pūtaiao me Te Ao Hangarau as part of the Spearhead Project: *Additive manufacturing and 3D and/or 4D printing of bio-composites*.

References

[1] R.M. Gorguluarslan, N. Gandhi Umesh, Y. Song, S.-K. Choi, An improved lattice structure design optimization framework considering additive manufacturing constraints, Rapid Prototyp. J. 23(2) (2017) 305-319.
[2] X. Mu, T. Bertron, C. Dunn, H. Qiao, J. Wu, Z. Zhao, C. Saldana, H.J. Qi, Porous polymeric materials by 3D printing of photocurable resin, Mater. Horizons 4(3) (2017) 442-449.
[3] D. Lei, Y. Yang, Z. Liu, S. Chen, B. Song, A. Shen, B. Yang, S. Li, Z. Yuan, Q. Qi, L. Sun, Y. Guo, H. Zuo, S. Huang, Q. Yang, X. Mo, C. He, B. Zhu, E.M. Jeffries, F.-L. Qing, X. Ye, Q. Zhao, Z. You, A general strategy of 3D printing thermosets for diverse applications, Mater. Horizons 6(2) (2019) 394-404.
[4] J. Yang, A.R. Webb, S.J. Pickerill, G. Hageman, G.A. Ameer, Synthesis and evaluation of poly(diol citrate) biodegradable elastomers, Biomaterials 27(9) (2006) 1889-1898.
[5] I. Djordjevic, N.R. Choudhury, N.K. Dutta, S. Kumar, Synthesis and characterization of novel citric acid-based polyester elastomers, Polymer 50(7) (2009) 1682-1691.
[6] A. Gleadall, I. Ashcroft, J. Segal, VOLCO: A predictive model for 3D printed microarchitecture, Addit. Manuf. 21 (2018) 605-618.
[7] S. Mohanty, K. Sanger, A. Heiskanen, J. Trifol, P. Szabo, M. Dufva, J. Emnéus, A. Wolff, Fabrication of scalable tissue engineering scaffolds with dual-pore microarchitecture by combining 3D printing and particle leaching, Materials Science and Engineering: C 61 (2016) 180-189.
[8] M. Xu, G.M. Gratson, E.B. Duoss, R.F. Shepherd, J.A. Lewis, Biomimetic silicification of 3D polyamine-rich scaffolds assembled by direct ink writing, Soft Matter 2(3) (2006) 205-209.
[9] X. Xu, C.K.P. Vallabh, A. Krishnan, S. Volk, C. Cetinkaya, In-Process Thread Orientation Monitoring in Additive Manufacturing, 3D Print. Addit. Manuf. 6(1) (2019) 21-30.
[10] J. Maurath, N. Willenbacher, 3D printing of open-porous cellular ceramics with high specific strength, J. Eur. Ceram. Soc. 37(15) (2017) 4833-4842.
[11] J.A. Lewis, J.E. Smay, J. Stuecker, J. Cesarano, Direct ink writing of three-dimensional ceramic structures, Journal of the American Ceramic Society 89(12) (2006) 3599-3609.
[12] K. Seunarine, N. Gadegaard, M. Tormen, D.O. Meredith, M.O. Riehle, C.D.W. Wilkinson, 3D polymer scaffolds for tissue engineering, Nanomedicine 1(3) (2006) 281-96.
[13] C.D. O'Connell, C. Onofrillo, S. Duchi, X. Li, Y. Zhang, P. Tian, L. Lu, A. Trengove, A. Quigley, S. Gambhir, A. Khansari, T. Mladenovska, A. O'Connor, C. Di Bella, P.F. Choong, G.G. Wallace, Evaluation of sterilisation methods for bio-ink components: gelatin, gelatin methacryloyl, hyaluronic acid and hyaluronic acid methacryloyl, Biofabrication 11(3) (2019) 035003.
[14] J.N. Hanson Shepherd, S.T. Parker, R.F. Shepherd, M.U. Gillette, J.A. Lewis, R.G. Nuzzo, 3D Microperiodic Hydrogel Scaffolds for Robust Neuronal Cultures, Adv. Funct. Mater. 21(1) (2011) 47-54.
[15] S. Ebnesajjad, Handbook of Biopolymers and Biodegradable Plastics : Properties, Processing and Applications, Elsevier Science & Technology Books, St. Louis, USA, 2012.
[16] A.P. Mathew, G. Gong, N. Bjorngrim, D. Wixe, K. Oksman, Moisture absorption behavior and its impact on the mechanical properties of cellulose whiskers-based polyvinylacetate nanocomposites, Polym. Eng. Sci. 51(11) (2011) 2136-2142.
[17] M.J. Lundahl, A.G. Cunha, E. Rojo, A.C. Papageorgiou, L. Rautkari, J.C. Arboleda, O.J. Rojas, Strength and water interactions of cellulose I filaments wet-spun from cellulose nanofibril hydrogels, Sci. Rep. 6 (2016) 30695.
[18] A. Sydney Gladman, E.A. Matsumoto, R.G. Nuzzo, L. Mahadevan, J.A. Lewis, Biomimetic 4D printing, Nat. Mater. 15(4) (2016) 413-418.
[19] S.I. Hong, W.Y. Choi, S.Y. Cho, S.H. Jung, B.Y. Shin, H.J. Park, Mechanical properties and biodegradability of poly-ε-caprolactone/soy protein isolate blends compatibilized by coconut oil, Polym. Degrad. Stab. 94(10) (2009) 1876-1881.
[20] F. Seniha Güner, Y. Yağcı, A. Tuncer Erciyes, Polymers from triglyceride oils, Prog. Polym. Sci. 31(7) (2006) 633-670.
[21] B. Tisserat, R.H. O'Kuru, H. Hwang, A.A. Mohamed, R. Holser, Glycerol citrate polyesters produced through heating without catalysis, J. Appl. Polym. Sci. 125(5) (2012) 3429-3437.
[22] Q.-Y. Liu, S.-Z. Wu, T.-W. Tan, J.-Y. Weng, L.-Q. Zhang, L. Liu, W. Tian, D.-F. Chen, Preparation and properties of a novel biodegradable polyester elastomer with functional groups, Journal of Biomaterials Science, Polymer Edition 20(11) (2009) 1567-1578.

[23] D. Pramanick, T.T. Ray, Synthesis and biodegradation of copolyesters from citric acid and glycerol, Polym. Bull. 19(4) (1988) 365-370.
[24] C. Briody, B. Duignan, S. Jerrams, J. Tiernan, The implementation of a visco-hyperelastic numerical material model for simulating the behaviour of polymer foam materials, Computational Materials Science 64 (2012) 47-51.
[25] ASTM International, D1621 − 10 Standard Test Method for Compressive Properties of Rigid Cellular Plastics, USA, 2010.
[26] L.J. Gibson, M.F. Ashby, Cellular solids : structure and properties, 2nd ed., Cambridge University Press, UK, 1997.
[27] D. Whisler, H. Kim, Experimental and simulated high strain dynamic loading of polyurethane foam, Polym. Test. 41 (2015) 219-230.
[28] R. Gümrük, R.A.W. Mines, Compressive behaviour of stainless steel micro-lattice structures, Int. J. Mech. Sci. 68 (2013) 125-139.
[29] A. Surmiri, K. Hasanpour, A new hardening rule for metallic foam plasticity, J. Mech. Sci. Technol. 30(5) (2016) 2105-2111.
[30] S. Kim, H. Shin, S. Rhim, K.Y. Rhee, Calibration of hyperelastic and hyperfoam constitutive models for an indentation event of rigid polyurethane foam, Compos. B. Eng. 163 (2019) 297-302.
[31] C. Briody, B. Duignan, S. Jerrams, Testing, modelling and validation of numerical model capable of predicting stress fields throughout polyurethane foam, 7th European Conference on Constitutive models for Rubber, 2011, p. 143.
[32] G. Siqueira, D. Kokkinis, R. Libanori, M.K. Hausmann, A.S. Gladman, A. Neels, P. Tingaut, T. Zimmermann, J.A. Lewis, A.R. Studart, Cellulose nanocrystal inks for 3D printing of textured cellular architectures, Adv. Funct. Mater. 27(12) (2017) 1604619-n/a.
[33] K. Oksman, Y. Aitomäki, A.P. Mathew, G. Siqueira, Q. Zhou, S. Butylina, S. Tanpichai, X. Zhou, S. Hooshmand, Review of the recent developments in cellulose nanocomposite processing, Compos. Part A Appl. Sci. Manuf. 83 (2016) 2-18.
[34] K. Oksman, R.J. Moon, Characterization of Nanocomposites Structure, Handbook of Green Materials, World Scientific 2013, pp. 89-105.